Supporting Information

UV-induced Vesicle to Micelle Transition: A Mechanistic Study

Craig A. Machado, Roger Tran, Taylor A. Jenkins, Amanda M. Pritzlaff, Michael B. Sims, Brent S. Sumerlin, Daniel A. Savin*

George & Josephine Butler Polymer Research Laboratory, Center for Macromolecular Science & Engineering, Department of Chemistry, University of Florida, Gainesville, FL 32611, USA. E-mail: savin@chem.ufl.edu

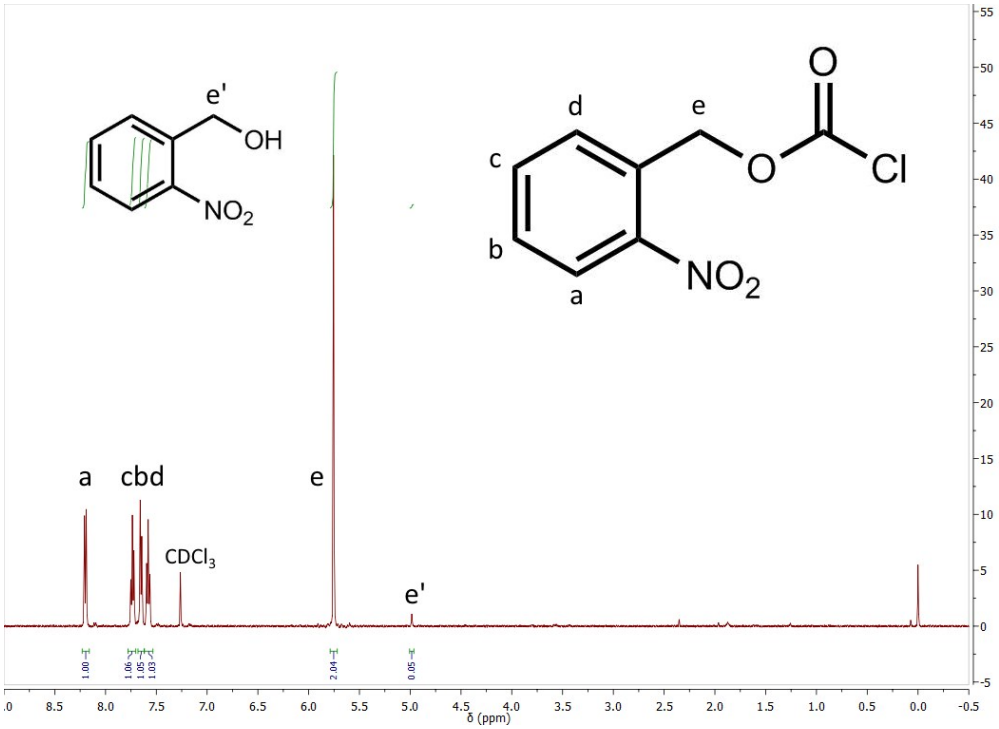

Figure S1. ^{1}H NMR spectrum of Nitrobenzyl Chloroformate

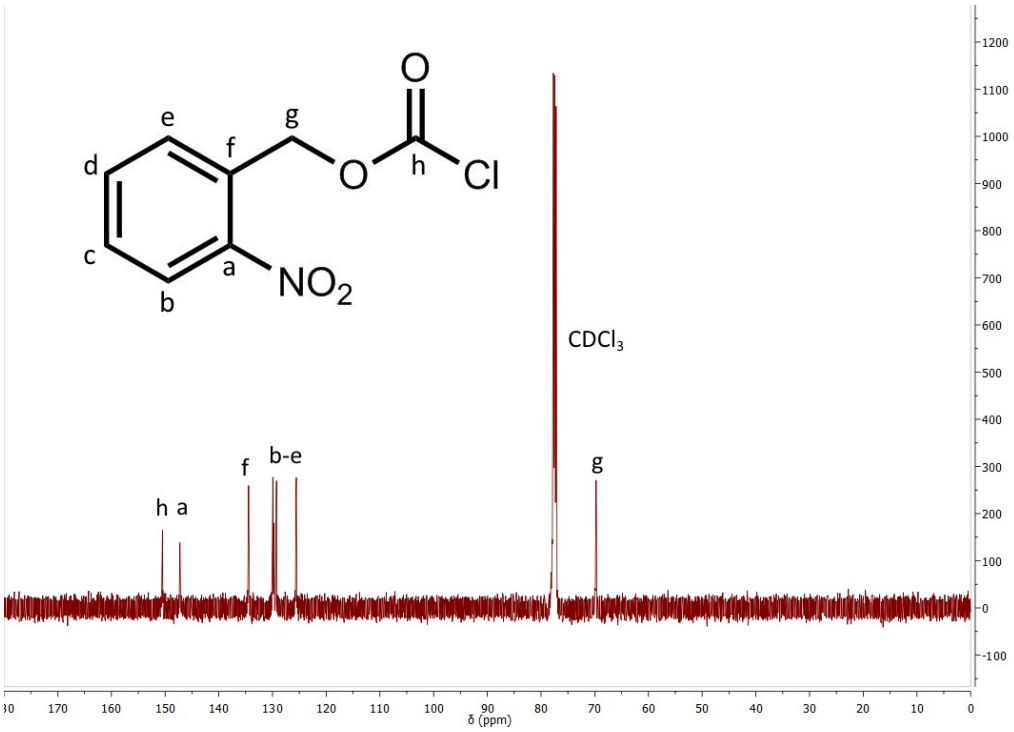

Figure S2. ^{13}C NMR spectrum of Nitrobenzyl Chloroformate

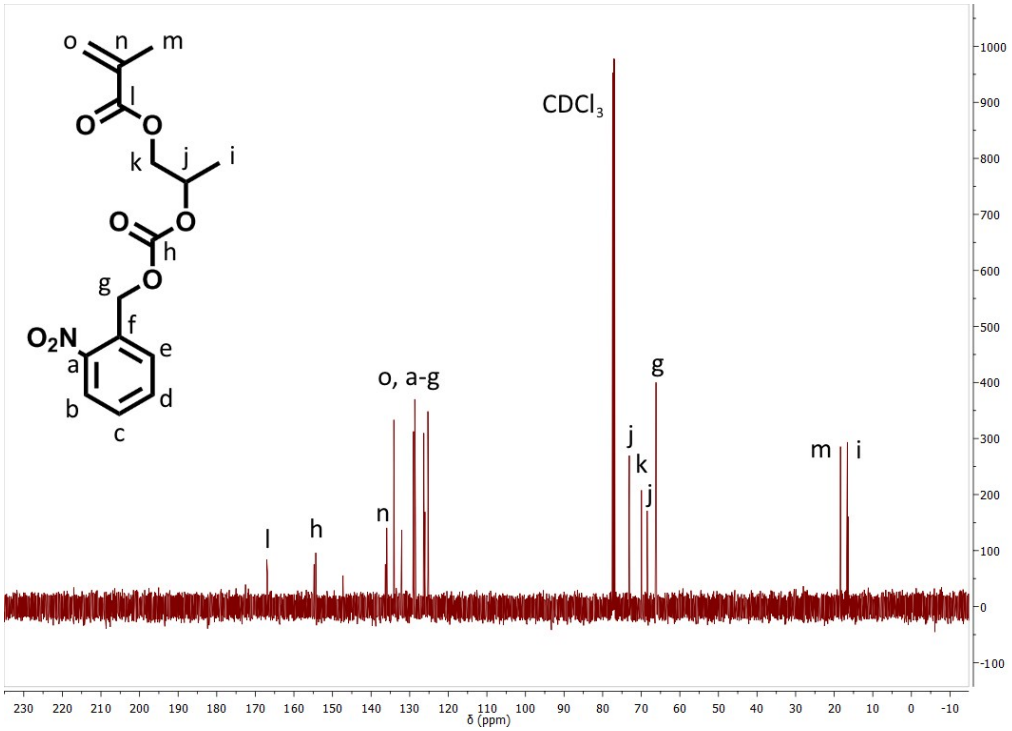

Figure S3. ^{13}C NMR spectrum of nitrobenzyl hydroxypropyl methacrylate

Mass Spectrometry and Liquid Chromatography Characterization of Monomer NbHPMA

Methods

High Resolution Mass Spectrometry (HRMS) and High Resolution LC-MS

HRMS and high resolution LC-MS were performed on an Agilent 6220 Time-of-Flight instrument. Monomers in solution were ionized via electrospray ionization (ESI) using a heated dry gas (N_2) for desolvation: flow rate – 8.0 L/min; gas temperature – 350 ºC, nebulization pressure – 30 psig. The injector was an Agilent 1100 series system (Santa Clara, CA) outfitted with a degasser (G13793), binary pump (G1312B), and auto sampler (G1367C). The mobile phase used for HRMS was methanol with 0.1% formic acid. The sample was prepared in methanol at an approximately 1 mg/mL concentration and was fully solubilized.

All LC-MS of NbHPMA was performed using a Thermo Scientific Hypersil GOLD C8 column (2.1 x 100 mm, 5 μm particle size), and mobile phases of water with 50 mM ammonium formate and 0.1% formic acid (mobile phase A) and methanol with 50 mM ammonium formate and 0.1% formic acid (mobile phase B) at a flow rate of 0.20 mL/min. Samples were separated using a gradient method starting at 10% B for 2 minutes, followed by a linear increase to 100% B at 15 minutes, and held at 100% B for 10 minutes. The sample was prepared in water with 50 mM ammonium formate and 0.1% formic acid at an approximately 1 mg/mL concentration although not all sample dissolved.

Low Resolution LC-MS/MS and Direct Infusion MS

LC-MS/MS with fragmentation by collision induced dissociation (CID) and direct infusion mass spectrometry of NbHPMA were performed on a Thermo Fisher Scientific LTQ XL Linear Ion Trap Mass Spectrometer. An electrospray ionization (ESI) ionization source was used with a heated dry gas (N_2) for desolvation. ESI method parameters included: N_2 sheath gas = 7 (unit less), N_2 aux gas = 0 (unit less), capillary temperature = 300°C, and spray voltage of 5kV. Fragmentation (MS2) was performed using an isolation width of *m/z* 4.0, normalized collision energy (NCE) of 35%, an activation q of 0.250, and a detection range of *m/z* 100-1200. For direct infusion MS, the sample was prepared in methanol at an approximately 1 mg/mL concentration. For LC-MS/MS, the mobile phases, gradient parameters, and sample preparation matched those listed above for high resolution LC-MS.

Characterization Data

HRMS Accurate Mass Confirmation of NbHPMA

The molecular formula of NbHPMA was confirmed using HRMS with a mass error of 4.1 ppm using the $[M+NH_4]^+$ ion labeled in Figure S4 (Theoretical mass = *m/z* 341.1343). Peaks present at *m/z* 369 and 127 were reproducibly observed in replicate injections.

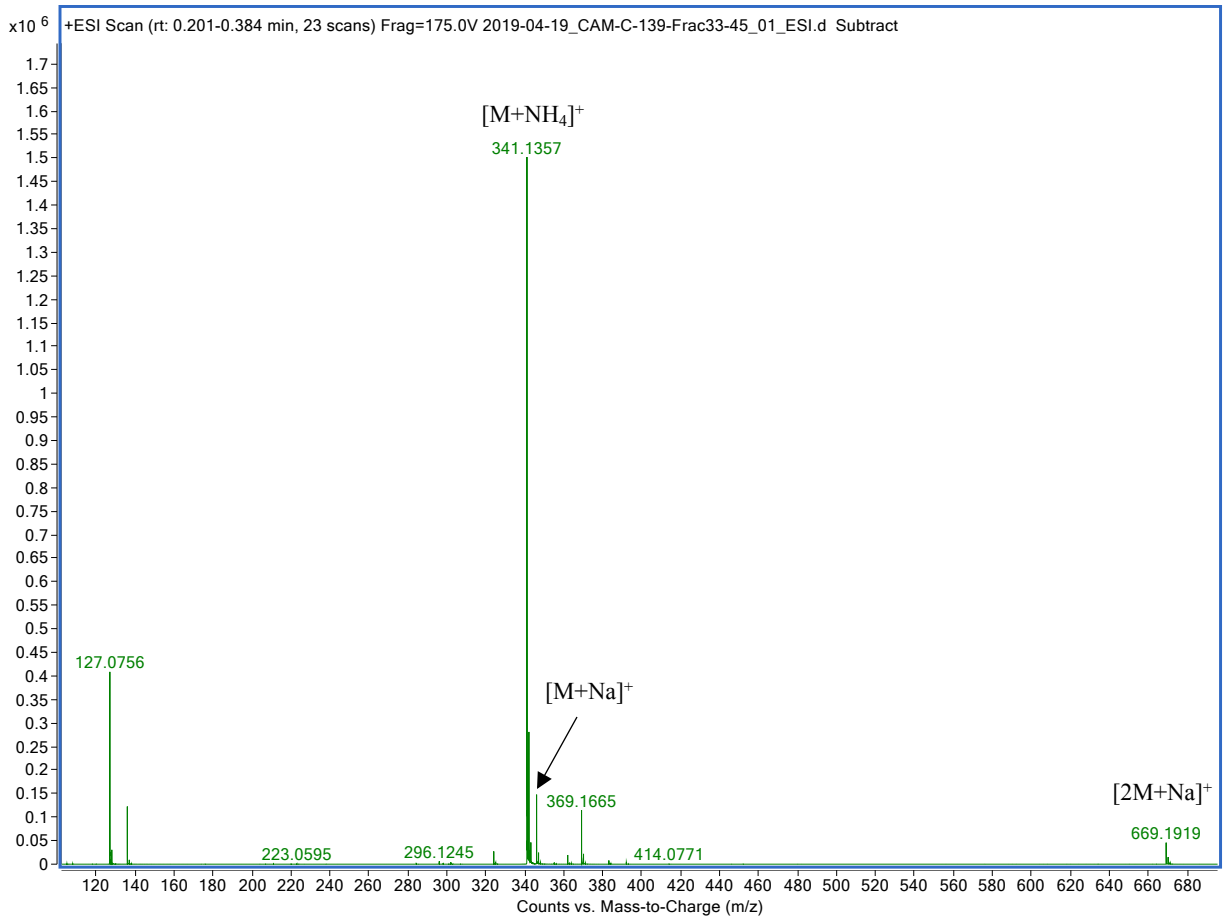

Figure S4. HRMS of NbHPMA. The indicated peak at *m/z* 341.1357 represents the $[M+NH4]^+$ adduct of NbHPMA. $[M+Na]^+$ is indicated at *m/z* 346.0902.

High Resolution LC-MS to Determine Purity of NbHPMA

High resolution LC-MS of NbHPMA was performed to determine purity of the sample and one peak was observed in the chromatogram suggesting a pure sample (Figure S5, top). The mass spectrum extracted from this peak is featured in Figure S6 and the predominant masses observed were *m/z* 341, 369, and 664. The masses *m/z* 341 and 664 were the sample related ions $[M+NH_4]^+$ and $[2M+NH_4]^+$, respectively. The impurity at *m/z* 369 was suspected to be sample-related due to co-elution with the NbHPMA $[M+NH_4]^+$ ion at *m/z* 341. This is demonstrated by the overlapping extracted ion chromatograms (EIC) for each species in Figure S5 (*m/z* 341 (middle, red) and *m/z* 369 (bottom, green)).

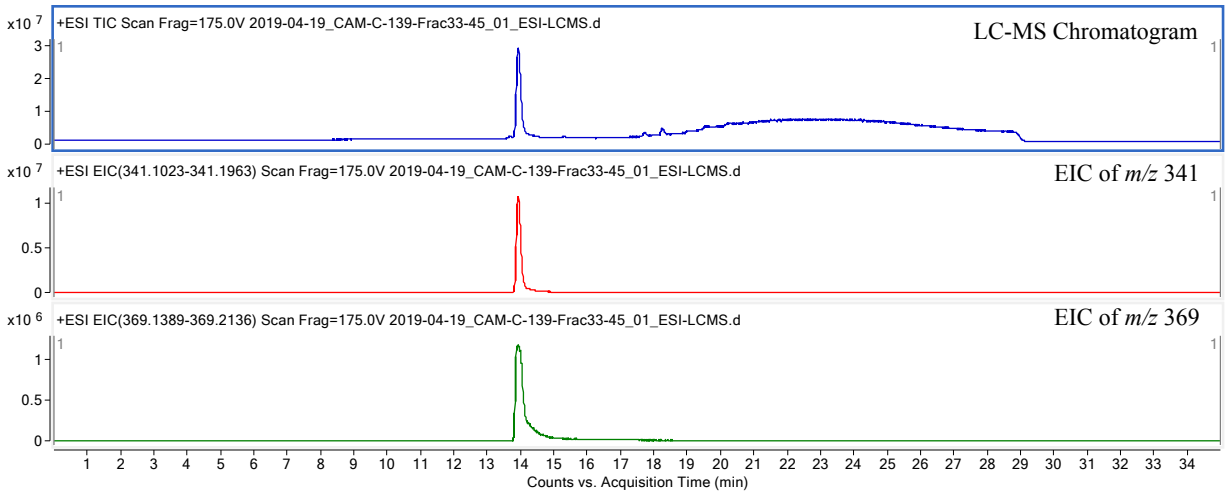

Figure S5. LC-MS chromatogram of NbHPMA (top, blue) with an extracted ion chromatogram (EIC) of *m/z* 341 ($[M+NH_4]^+$ for NbHPMA) (middle, red) and an extracted ion chromatogram for impurity *m/z* 369 (bottom, green).

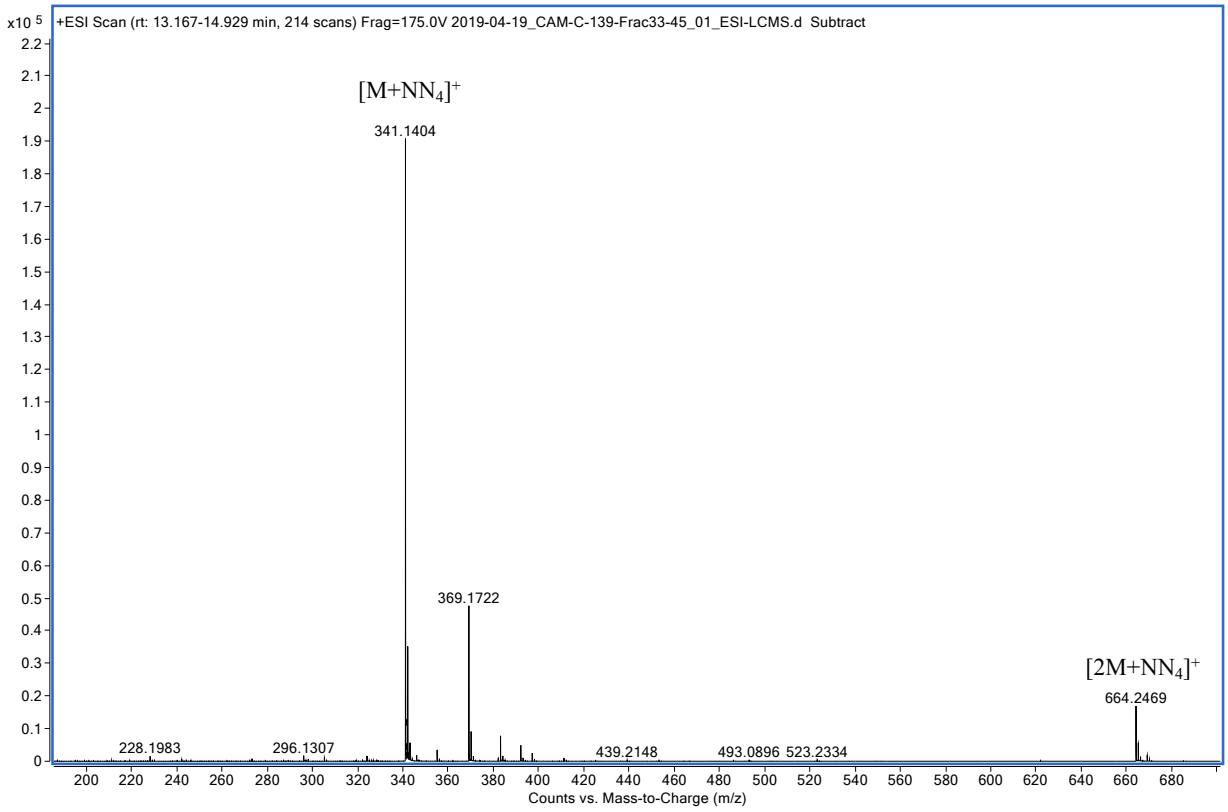

Figure S6. Mass spectrum of NbHPMA extracted from the single peak in the LC-MS chromatogram between 13.2 and 14.9 minutes.

CID Fragmentation Studies

To determine if the HRMS peak at *m/z* 369 was related to NbHPMA, low resolution LC-MS and CID fragmentation were performed with a Thermo Fisher Scientific LTQ XL Linear Ion Trap Mass Spectrometer (Figure S7). It was observed that the masses *m/z* 341 and 369 both decomposed into a fragment at *m/z* 127, which was also observable in the HRMS spectrum (Figure S4). The $[M+Na]^+$ peak for NbHPMA at *m/z* 346 was also fragmented and produced a daughter ion of *m/z* 127 (Figure S7). Two common fragment masses between *m/z* 341 and 369 were *m/z* 127 and 323 which suggested these masses were related and that *m/z* 369 can be included in overall sample purity.

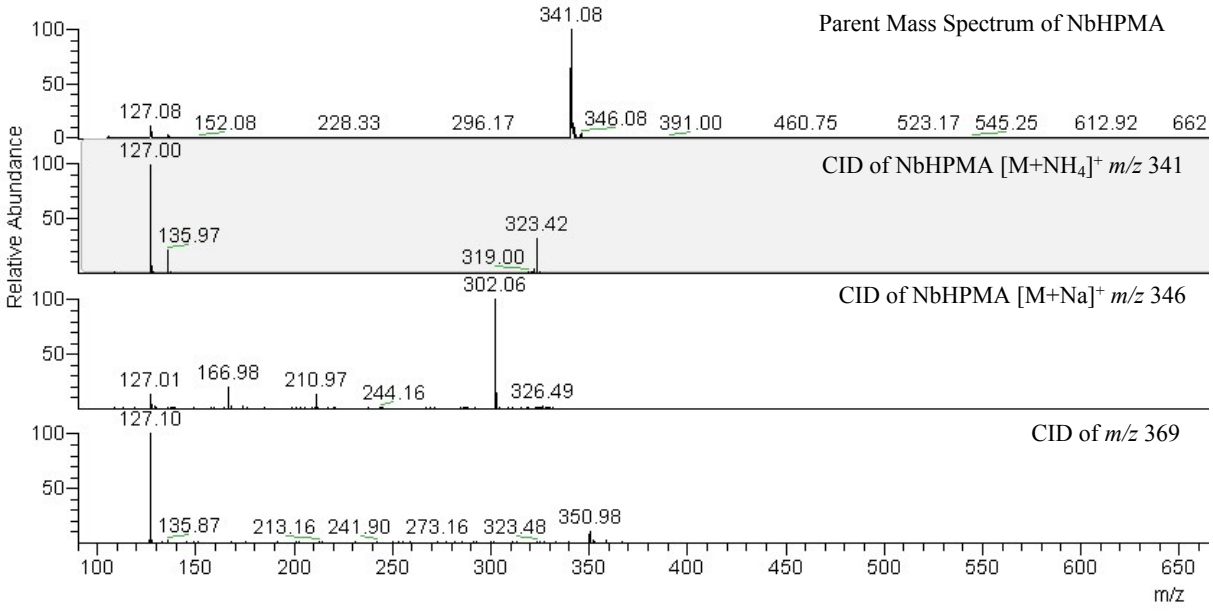

Figure S7. Parent mass spectrum of NbHPMA and fragmentation spectra (CID) of *m/z* 341, 346, and 369 (top to bottom).

Direct Injection MS of NbHPMA

Direct-infusion mass spectrometry, in which the sample is injected by syringe pump directly into the ESI ionization source, was employed to determine if *m/z* 369 was an artefact of the auto-injection process. The full mass spectrum shown in Figure S8 does not include m/z 369. **This result, combined with the results of the CID fragmentation study, suggested that *m/z* 369 was a derivative of NbHPMA formed during the auto sampler injection process prior to ionization.**

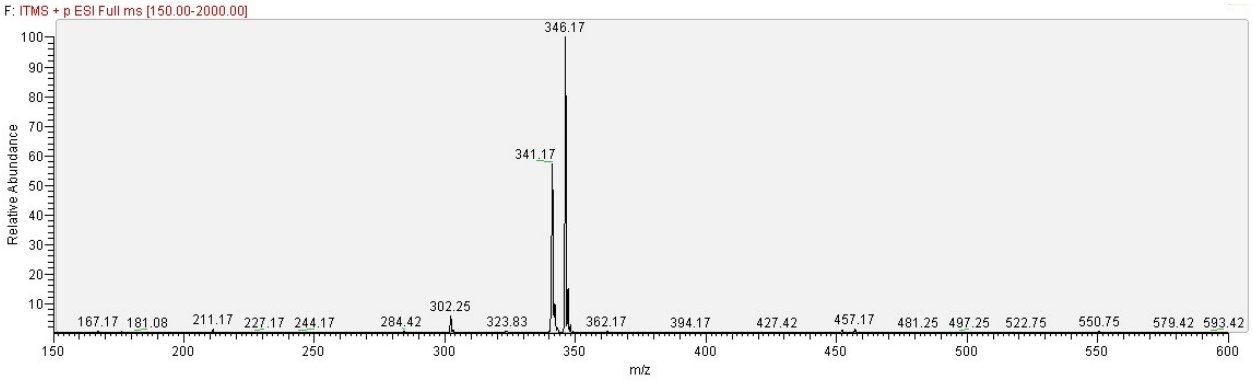

Figure S8. Low-resolution direct infusion mass spectrum of NbHPMA featuring high intensity peaks *m/z* 341 $[M+NH_4]^+$ and *m/z* 346 $[M+Na]^+$.

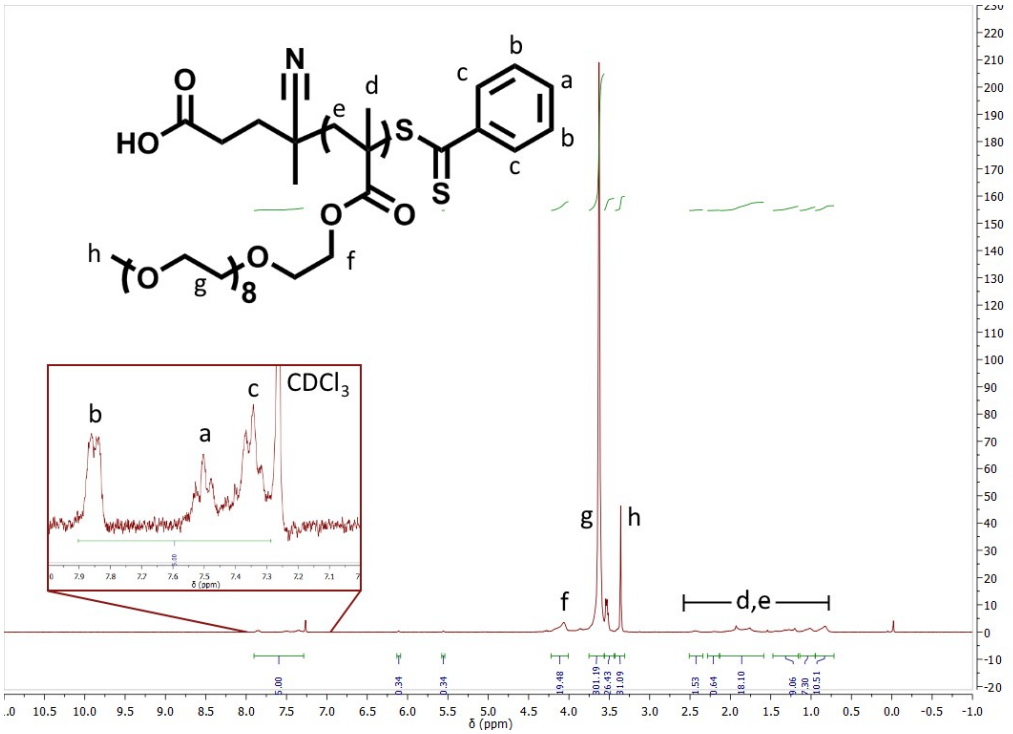

Figure S9. ^{1}H NMR spectrum of polyPEGMA

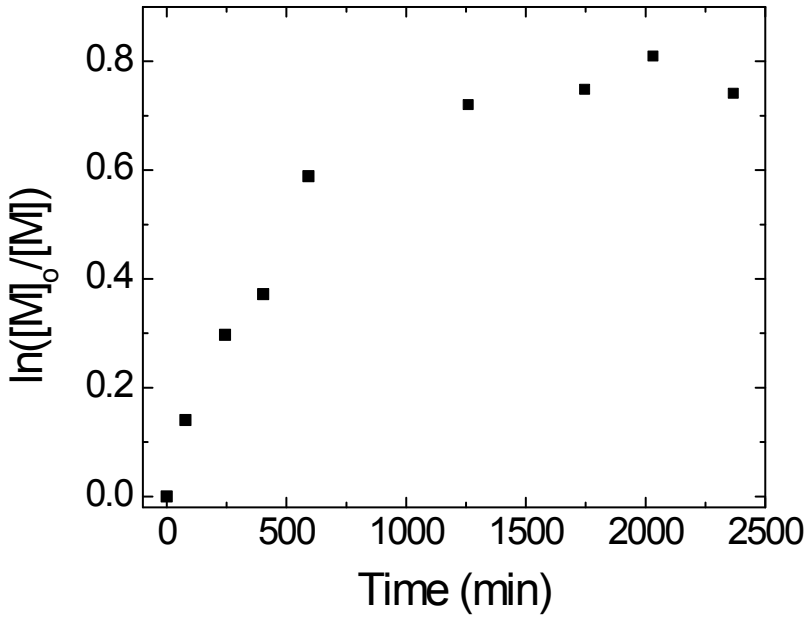

Figure S10. Pseudo-first order kinetic plot for initial block polymerization of PEGMA with NbHPMA at 70 °C. Plot is linear until 560 min, then has a decrease in slope, indicating the presence of termination events.

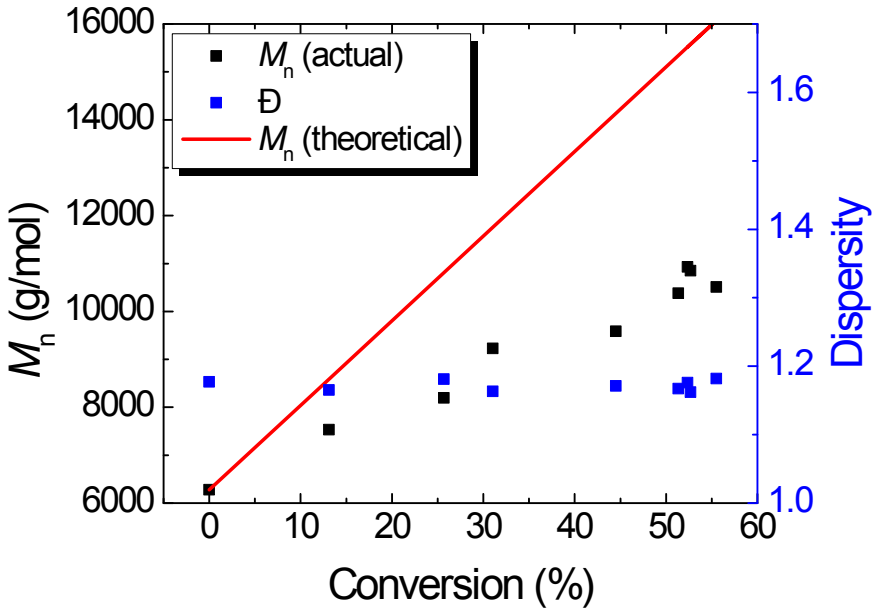

Figure S11. Plot of molecular weight and dispersity (determined *via* GPC against poly(methyl methacrylate) standards) as a function of conversion (determined *via* ^{1}H NMR) for initial block polymerization of PEGMA with NbHPMA at 70 °C.

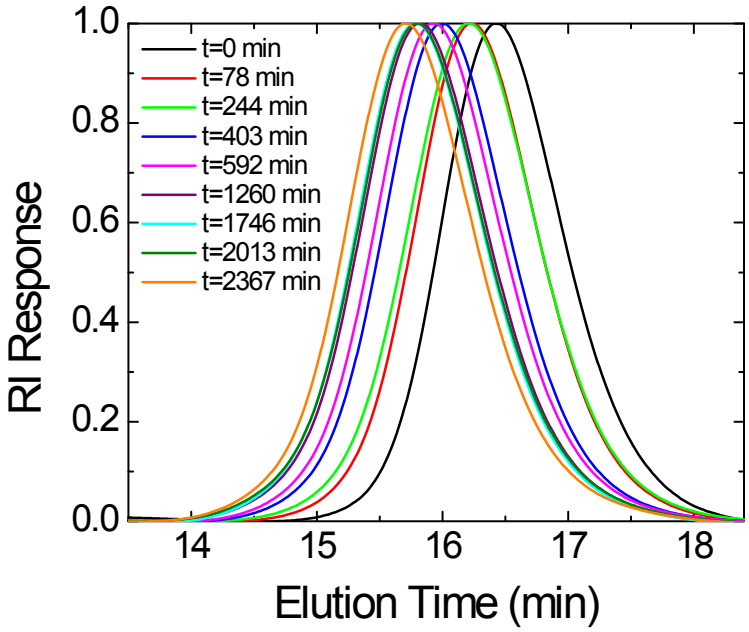

Figure S12. GPC traces of initial block polymerization 70 °C.

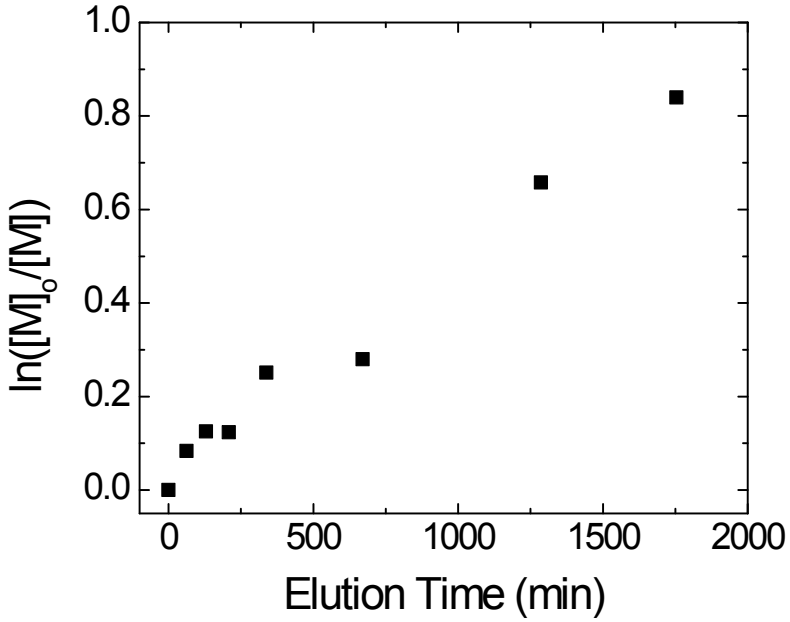

Figure S13. Linear pseudo-first order kinetic plot for poly(NbHPMA) polymerized at 70 °C.

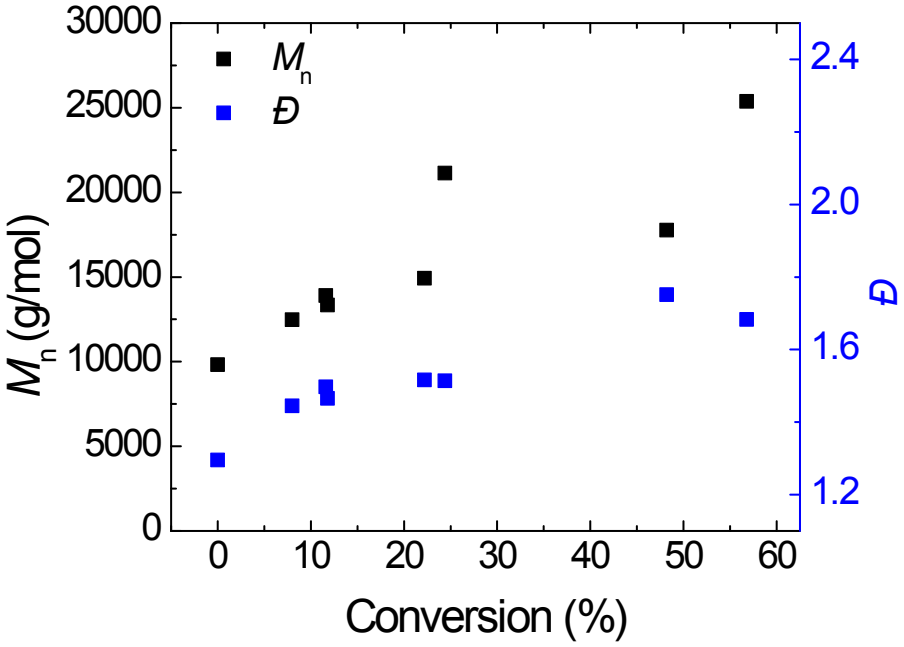

Figure S14. Plot of molecular weight and dispersity (determined *via* GPC against poly(methyl methacrylate) standards) as a function of conversion (determined *via* ^{1}H NMR) for poly(NbHPMA) polymerized at 70 °C.

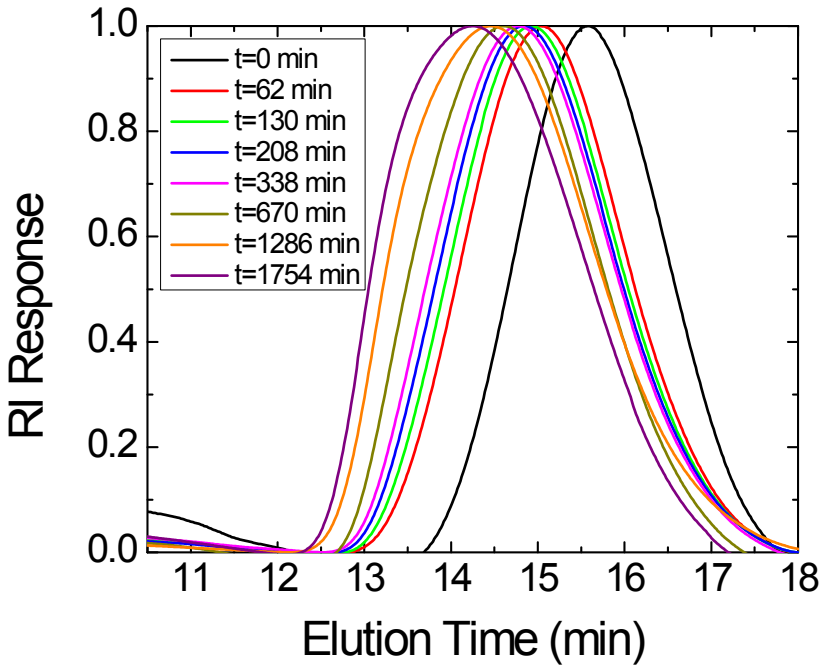

Figure S15. GPC traces of poly(NbHPMA) polymerized at 70 °C.

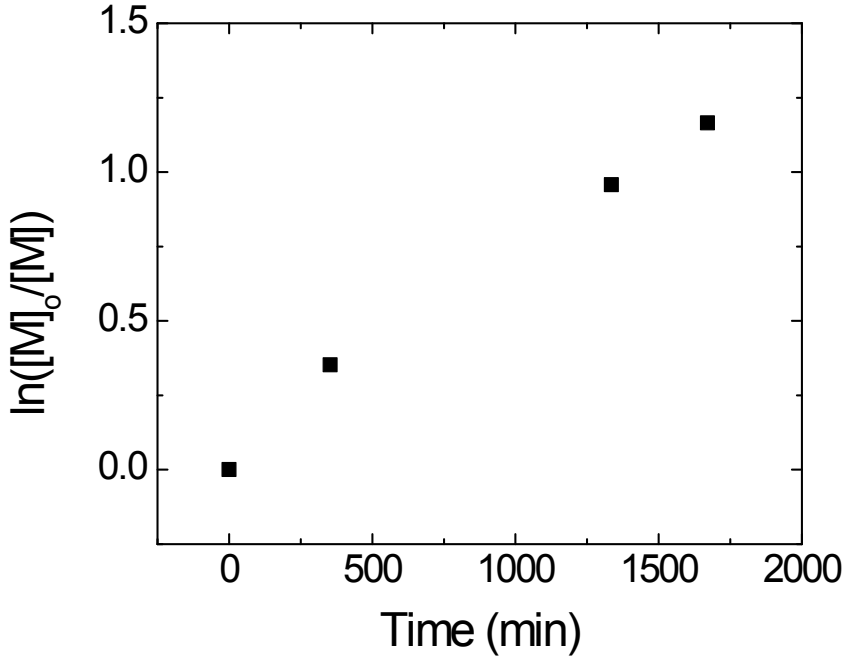

Figure S16. Linear pseudo-first order kinetic plot for poly(NbHPMA) polymerized at 35 °C.

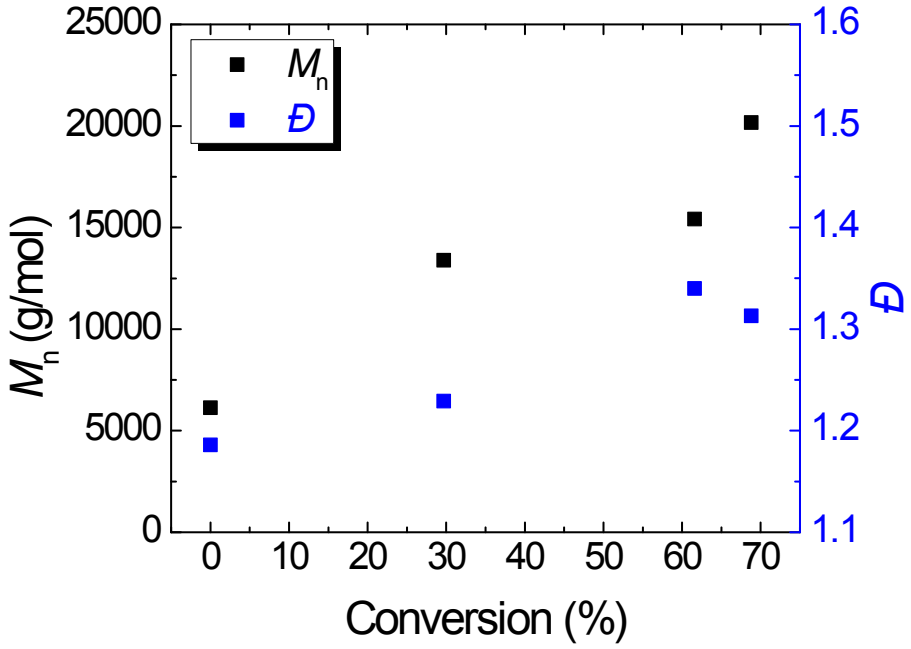

Figure S17. Plot of molecular weight and dispersity (determined *via* GPC against poly(methyl methacrylate) standards) as a function of conversion (determined *via* ^{1}H NMR) for poly(NbHPMA) polymerized at 35 °C.

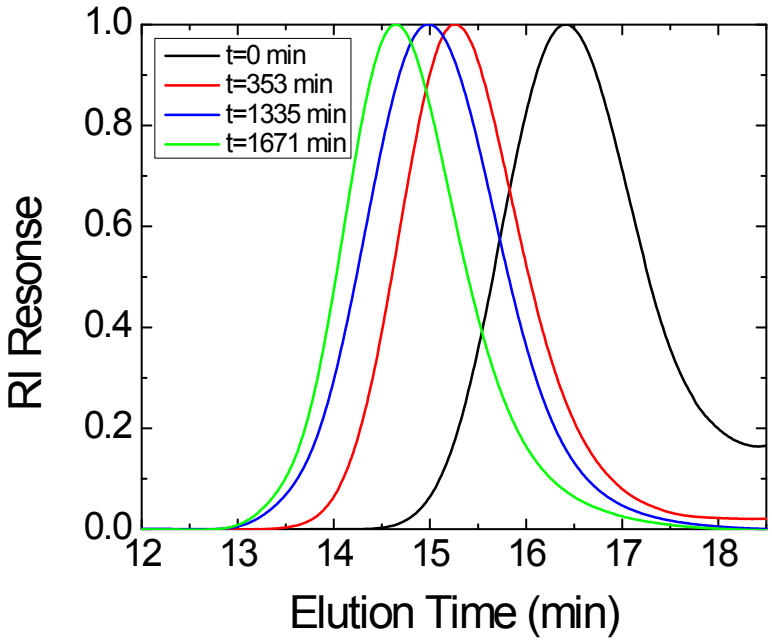

Figure S18. GPC traces of poly(NbHPMA) polymerized at 35 °C.

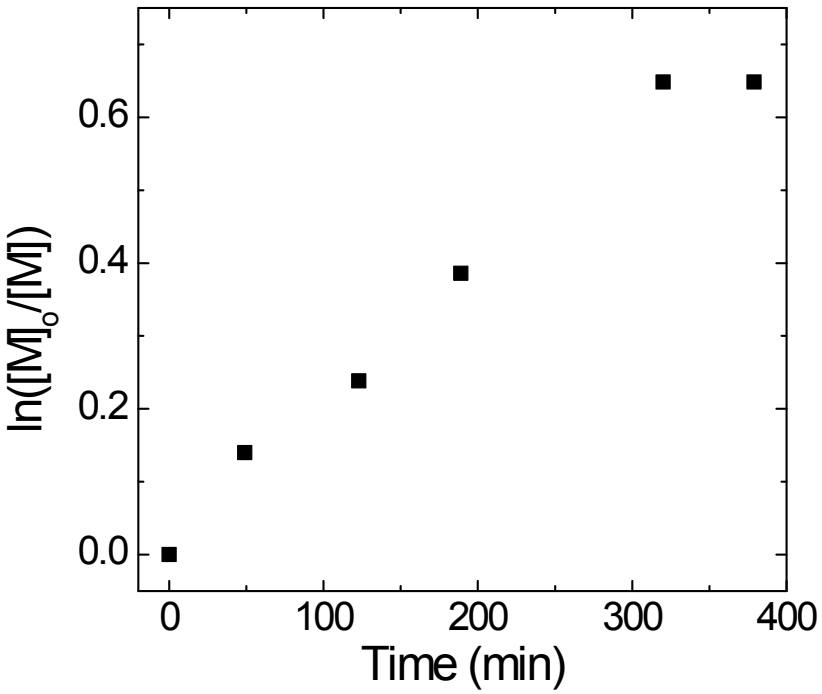

Figure S19. Linear pseudo-first order kinetic plot for Nb 94 polymerized at 35 °C.

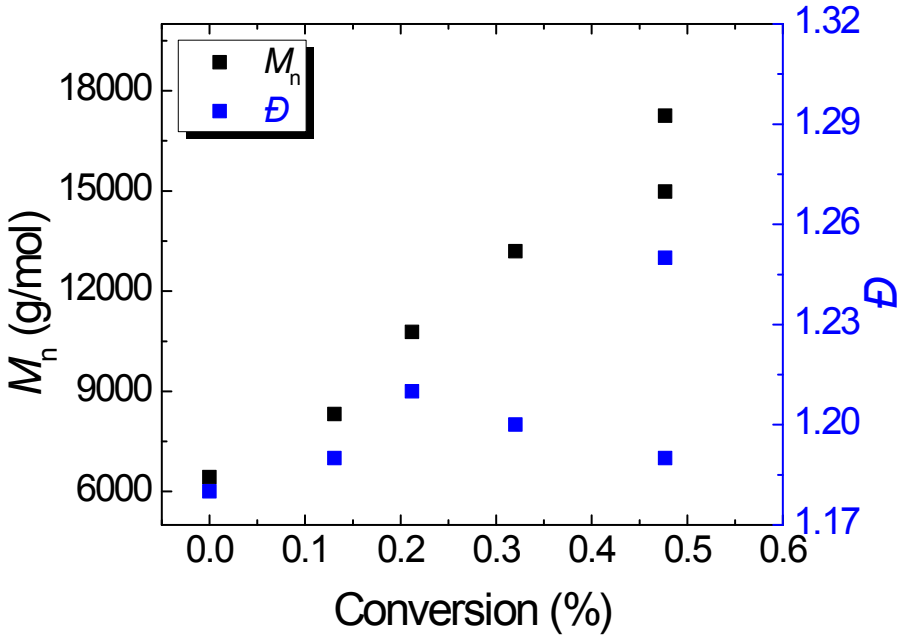

Figure S20. Plot of molecular weight and dispersity (determined *via* GPC against poly(methyl methacrylate) standards) as a function of conversion (determined *via* ^{1}H NMR) for Nb 94 polymerized at 35 °C.

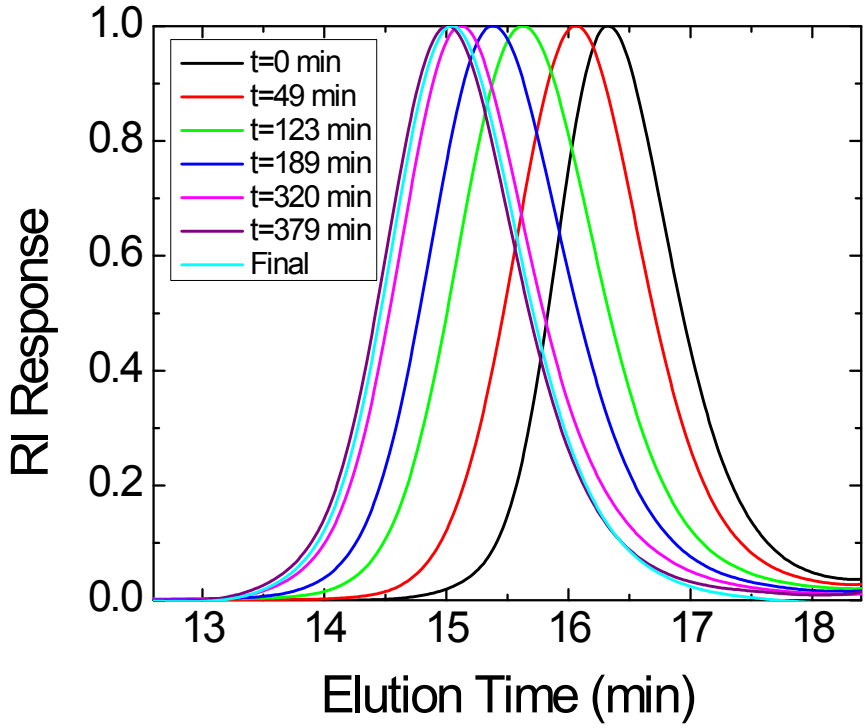

Figure S21. GPC traces of Nb 94 polymerized at 35 °C.

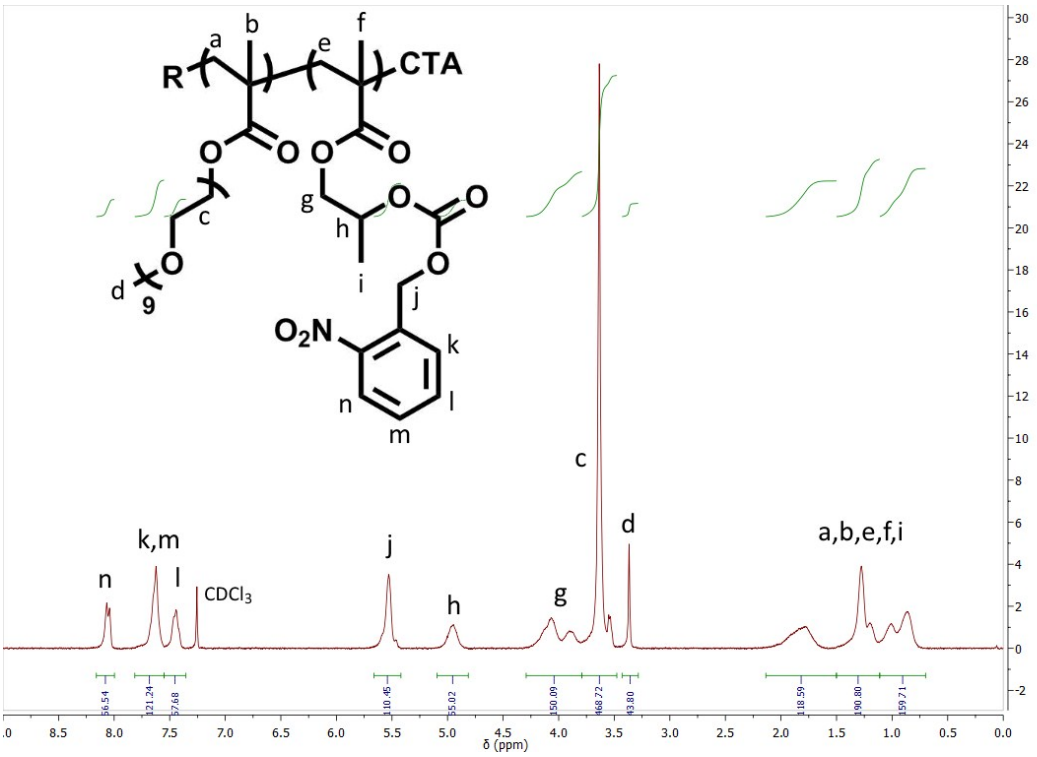

Figure S22. ^{1}H NMR of Nb 94.

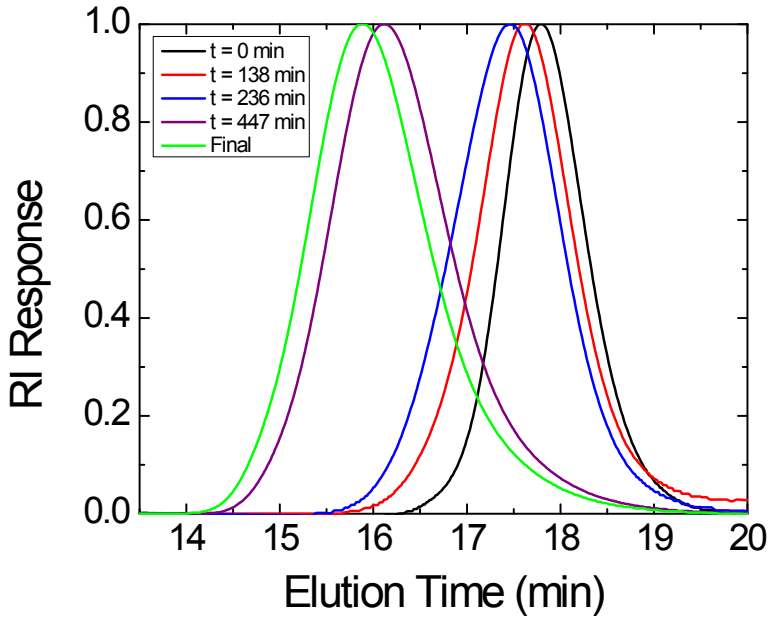

Figure S23. GPC traces of Nb 176 polymerized at 35 ^{o}C.

Note: Conversions at t = 138 and t=236 were too low to accurately measure *via* ^{1}H NMR (negative conversion was measured at t = 138), so kinetic plots involving conversion have been omitted.

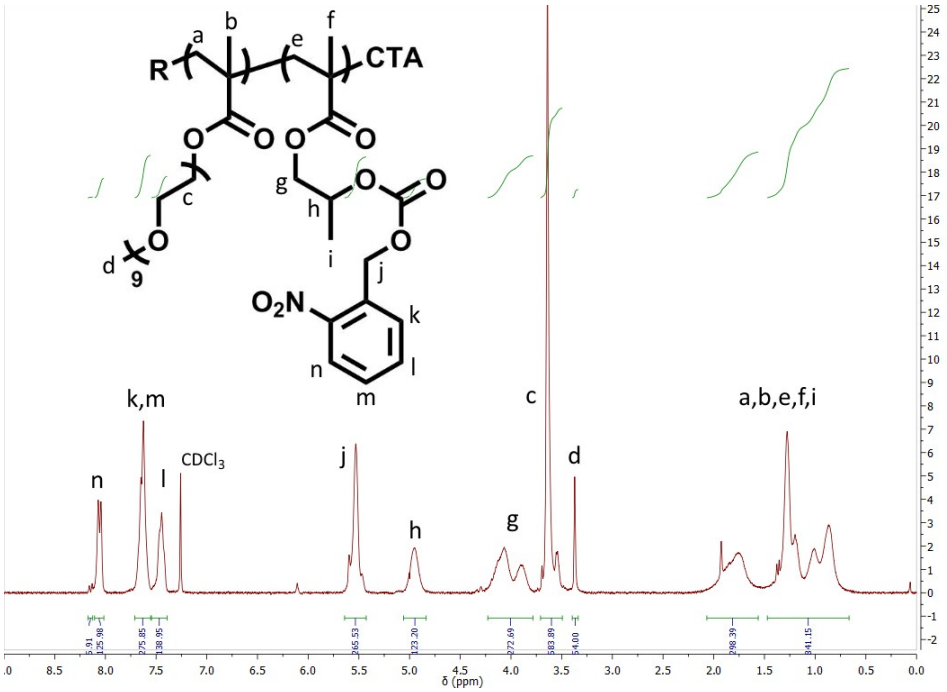

Figure S24. ^{1}H NMR of Nb 176.

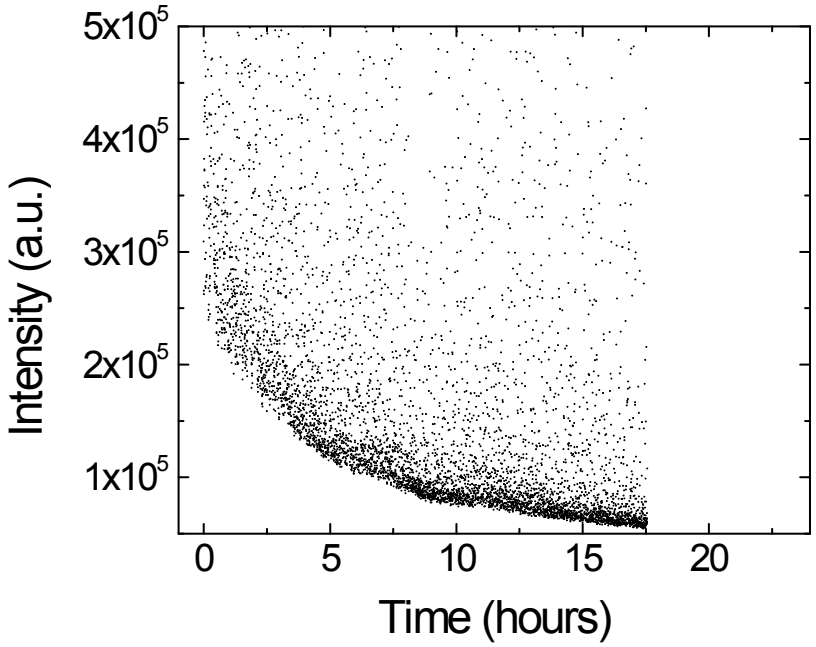

Figure S25. Scattered light intensity with crossed polarizers of Nb 94 solution as a function of time after 18 minutes of UV-irradiation. Due to the isotropic nature of the vesicles, very low light intensity reaches the detectors through the crossed polarizers, so the laser attenuation was adjusted accordingly. Spikes in intensity cause noise in the data, but the overall trend is the same as that in Figure 6.

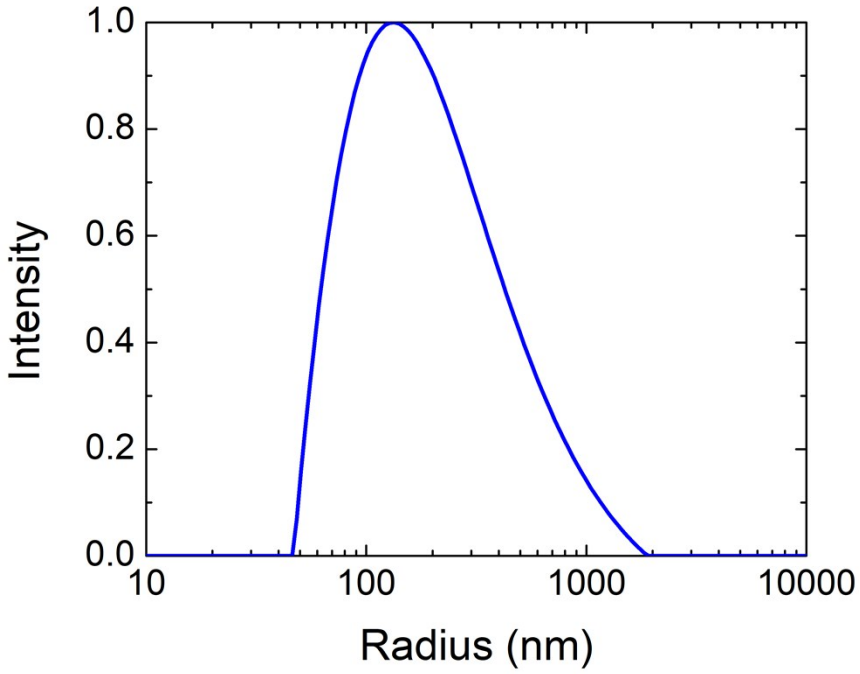

Figure S26. Representative CONTIN size distribution plot of Nb 94 assemblies prior to irradiation.

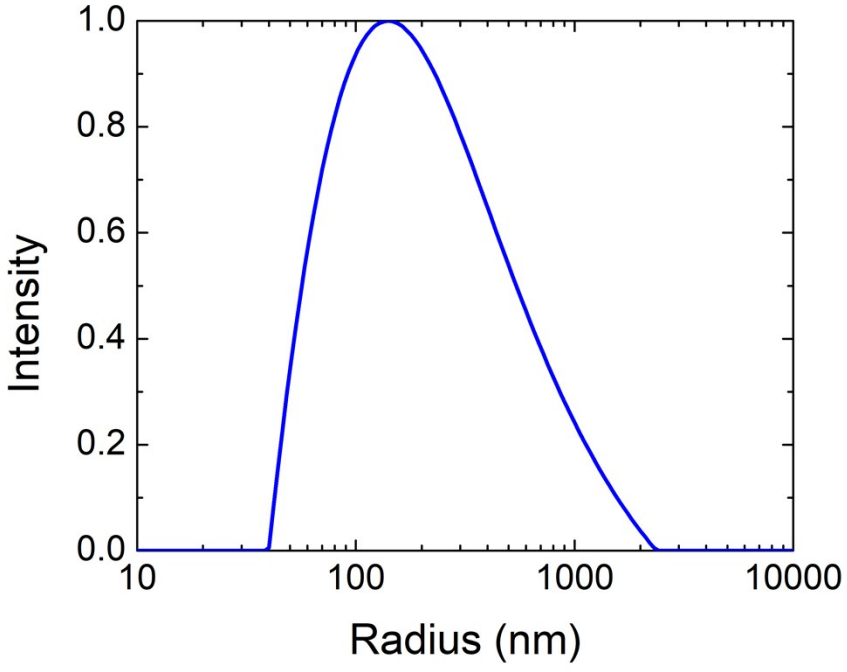

Figure S27. Representative CONTIN size distribution plot of Nb 94 assemblies after 100 min irradiation.

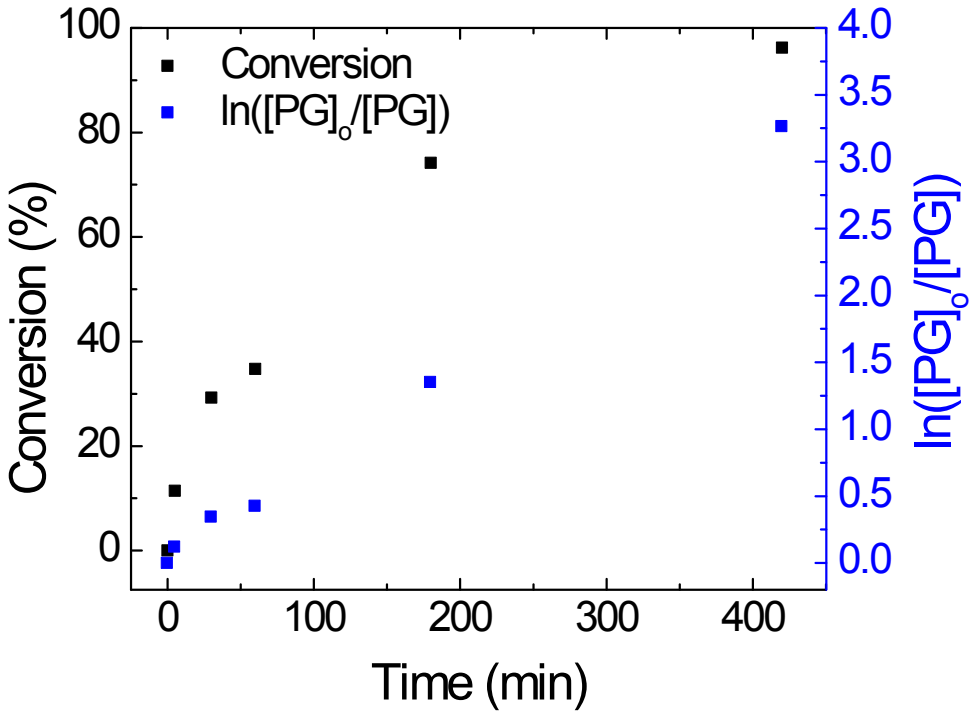

Figure S28. Kinetic plot of photolysis of preliminary block polymer. Block polymer was assembled in water and irradiated as detailed in experimental section. After given time intervals, aliquots were taken, solvent was removed, and ^{1}H NMR was used to quantify extent of photolysis of nitrobenzyl groups. Methoxy protons from PEGMA were integrated as 3H and the integration of phenyl peaks was used to quantify the residual protecting group (PG). The conversion of photolysis was plotted as a function of irradiation time and shows a logarithmic plateau (shown in black). The pseudo-first order kinetics appear linear for the process (shown in blue). After 7 hours of irradiation, over 96% of nitrobenzyl groups were cleaved.

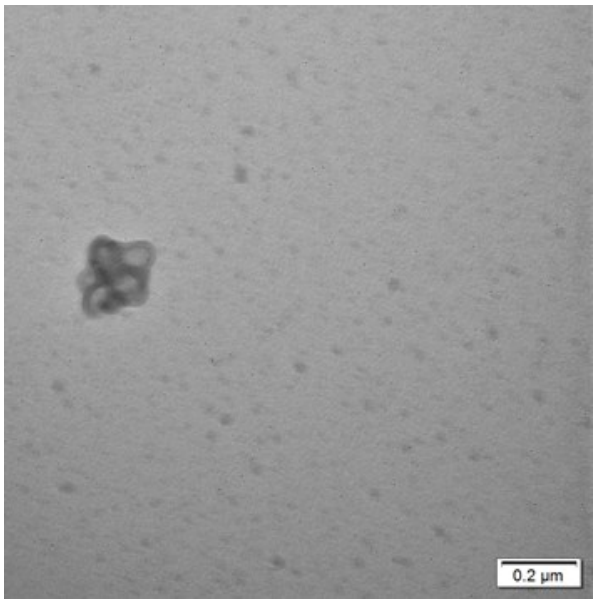

Figure S29. Image of a smaller Nb 176 assembly showing the fused vesicle morphology, indicating that the apparent bilayered appearance is not an artefact of focusing.

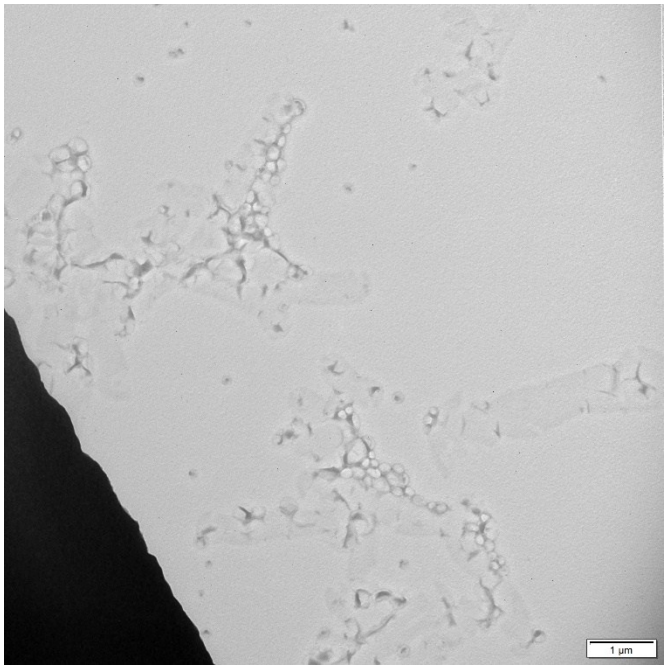

Figure S30. Additional TEM image of Nb 94 assemblies prior to irradiation, zoomed out to give a representative image of the assemblies.

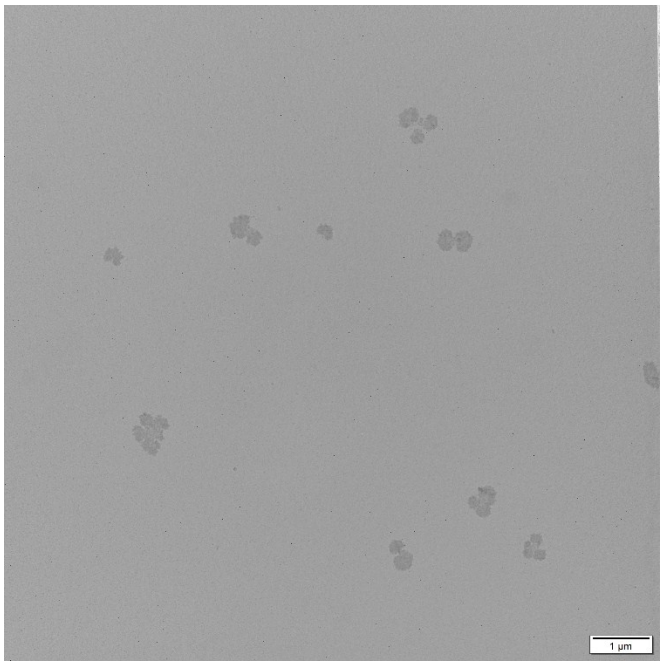

Figure S31. Additional TEM image of Nb 94 assemblies after 16 minutes of irradiation, zoomed out to give a representative image of the assemblies. Due to the complex shapes of the clover-like assemblies and the size agreement between DLS and TEM, we believe these assemblies are appear as they are in solution and are not a result of drying-induced-aggregation.

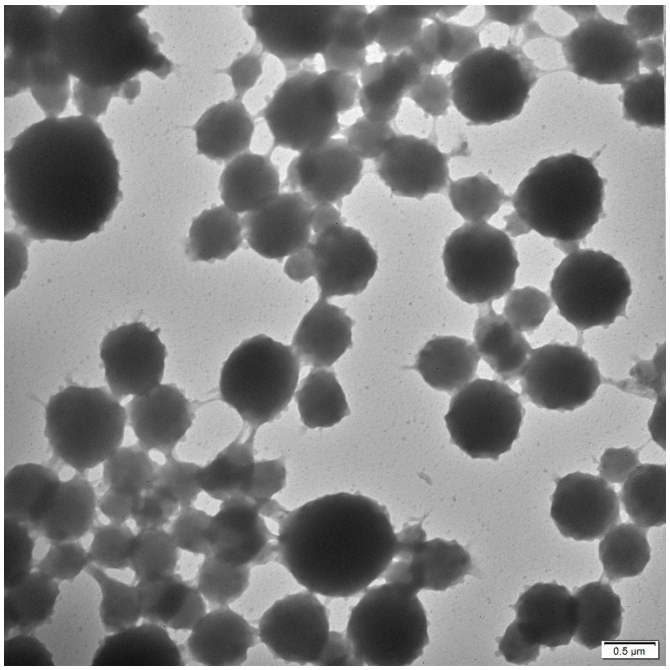

Figure S32. Additional TEM image of Nb 176 assemblies prior to irradiation, zoomed out to give a representative image of the assemblies. The bridges between the assemblies are likely an artifact of drying, based on R_h determined by DLS.

Table S1. Summary of self-assembly methods' effect on R_h for Nb 94.

Solvent	Method	R_h (nm)
THF	Dialysis	13
	Solvent Switch[1]	15
DMF	Solvent Switch[2]	438

Table S2. Summary of self-assembly methods' effect on R_h for Nb 176.

Solvent	Method	R_h (nm)
THF	Dialysis	34
	Solvent Switch[1]	24
	Solvent Switch[2]	13
Dioxane	Solvent Switch[2]	28
DMF	Solvent Switch[2]	973

[1]Polymer was dissolved at 0.1 mg/mL in organic solvent and water was added at 1 mL/hr. Organic solvent was allowed to evaporate under ambient conditions

[2]Polymer was dissolved at 20 mg/mL in organic solvent and water was added at 1.8 vol% per minute until an equal volume of water and organic solvent was achieved. The resultant solution was then dialyzed against deionized water.